Asteroid Density, Porosity, and Structure

D. T. Britt
University of Tennessee

D. Yeomans
NASA Jet Propulsion Laboratory

K. Housen
Boeing Aerospace

G. Consolmagno
Vatican Observatory

New data from observations of asteroid mutual perturbation events, observations of asteroid satellites, and spacecraft encounters have revolutionized our understanding of asteroid bulk density. Most asteroids appear to have bulk densities that are well below the grain density of their likely meteorite analogs. This indicates that many asteroids have significant porosity. High porosity attenuates shock propagation, strongly affecting the nature of cratering and greatly lengthening the collisional lifetimes of porous asteroids. Analysis of density trends suggests that asteroids are divided into three general groups: (1) asteroids that are essentially solid objects, (2) asteroids with macroporosities ~20% that are probably heavily fractured, and (3) asteroids with macroporosities >30% that are loosely consolidated "rubble pile" structures.

1. OVERVIEW: THE DENSITY AND POROSITY OF ASTEROIDS

Data from a number of sources indicate that many asteroids have significant porosity. In some cases, porosities are large enough to affect asteroid internal structure, gravity field, impact dynamics, and collisional lifetimes. Porosity can also affect a range of asteroid physical properties including thermal diffusivity, seismic velocity, cosmic-ray exposure, and dielectric permeability. The thermal and seismic effects can in turn affect asteroid internal evolution, metamorphism, shock dissipation, and elastic properties, which can determine whether colliding asteroids accrete or disrupt. The study of asteroid bulk density, along with supporting studies of meteorite porosity and physical properties, is just beginning. These data allow for new views of asteroid belt structure and evolution. This chapter will review some of the basic data accumulated on asteroid bulk density and meteorite grain densities. Using these data we will estimate the porosities of asteroids, outline the implications of high porosity on internal structure, examine how porous asteroids respond to impacts and shock, and interpret these data to characterize the distribution of porous objects in the asteroid belt.

1.1. Terms and Definitions

Density, expressed as mass per unit volume, is a fundamental physical property of matter. For common rock-forming minerals, the crystal structures, lattice volumes, and elemental compositions are well defined, so the densities of geologic materials common in asteroids are similarly well defined. Examples of these densities include 2.2–2.6 g/cm^3 for clays, 3.2–4.37 g/cm^3 for the mafic silicates pyroxene and olivine, and 7.3–7.7 g/cm^3 for Ni-Fe. These densities refer to a grain density, which is the mass of an object divided by the volume occupied only by mineral grains. This is the average density of the solid portions of a rock. The density value returned by spacecraft measurements is bulk density, which is the mass of an object divided by its volume (including the volume of its pore spaces). The ratio between grain and bulk density is the porosity, the percentage of the bulk volume of a rock that is occupied by empty space. Porosity can be a major component of asteroid volume, and some porosity is found in most meteorites. The type of porosity measured in meteorites is microporosity, which is the meteorite's fractures, voids, and pores on the scale of tens of micrometers. Microporosity is subject to strong selection effects since these features cannot be so large or thoroughgoing as to prevent the meteorite from surviving transport to Earth. Microporosity can represent both voids and pores that have survived from the earliest formation of these aggregates as well as post-lithification impact-induced fractures. Both types have been reported in scanning electron microscopy (SEM) studies of a limited number of meteorite thin sections, but at least in ordinary chondrites it appears that impact fractures dominate (*Flynn et al.,* 1999; *Consolmagno et al.,* 1999). Large-scale voids and fractures on asteroids are called macroporosity and are probably produced by the impact history of the asteroid. These are features that are large on the scale of meteorites and are the zones of struc-

TABLE 1. Asteroid bulk density measurements: A compilation of current data on asteroid mass, volume, and bulk density.

Asteroid	Mass (10^{-10} $M_\odot$)	Mass (10^{19} kg)	Diameter (km)	Bulk Density (g/cm^3)	References
1 Ceres (G)	4.762 ± 0.015	94.7	948.8 ± 11.2	2.12 ± 0.04	*Standish* (2001), *Drummond et al.* (1998)
	4.70 ± 0.04	93.5			*Michalak* (2000)
	4.39 ± 0.04	87.3			*Hilton* (1999)
	4.70	93.5			*Standish* (1998)
	4.759 ± 0.023	94.7			*Viateau and Rapaport* (1998)
	5.0 ± 0.2	99			*Viateau and Rapaport* (1995)
		103			*Hilton et al.* (1996)
	4.74 ± 0.3	94			*Goffin* (1991)
	5.0 ± 0.2	99			*Standish and Hellings* (1989)
	5.21 ± 0.3	103			*Landgraf* (1988)
	5.9 ± 0.3	117			*Schubart and Matson* (1979)
			848.4 ± 19.7		*Tedesco et al.* (1992)
			941.4 ± 34		*Millis et al.* (1987)
2 Pallas (B)	1.078 ± 0.038	21.4	532.6 ± 6	2.71 ± 0.11	*Standish* (2001), *Dunham et al.* (1990)
	1.17 ± 0.03	23.3			*Goffin* (2001)
	1.21 ± 0.26	24.1			*Michalak* (2000)
	1.59 ± 0.05	31.6			*Hilton* (1999)
	1.00	21.4			*Standish* (1998)
	1.4 ± 0.2	28			*Standish and Hellings* (1989)
	1.08 ± 0.22	21	538		*Schubart and Matson* (1979)
			498.1 ± 18.8		*Tedesco et al.* (1992)
			538 ± 12		*Wasserman et al.* (1979)
			524.4 ± 15.2		*Drummond and Cocke* (1989)
4 Vesta (V)	1.341 ± 0.015	26.7	529 ± 10	3.44 ± 0.12	*Standish* (2001), *Thomas et al.* (1997)
	1.36 ± 0.05	27.0			*Michalak* (2000)
	1.69 ± 0.11	34			*Hilton* (1999)
	1.30	25.9			*Standish* (1998)
	1.33	26			*Goffin* (1991)
	1.5 ± 0.3	30			*Standish and Hellings* (1989)
	1.38 ± 0.12	27	525		*Schubart and Matson* (1979)
	1.17 ± 0.10	23			*Hertz* (1966)
			468.3 ± 26.7		*Tedesco et al.* (1992)
10 Hygeia (C)	0.49 ± 0.21	10	407.1 ± 6.8	2.76 ± 1.2	*Goffin* (1991), *Tedesco et al.* (1992)
	0.47 ± 0.23	9			*Scholl et al.* (1987)
11 Parthenope (S)	0.0258 ± 0.001	0.513	153.3 ± 3.1	2.72 ± 0.12	*Viateau and Rapaport* (1997), *Tedesco et al.* (1992)
15 Eunomia (S)	0.042 ± 0.011	0.84	255.3 ± 15.0	0.96 ± 0.3	*Hilton* (1997), *Tedesco et al.* (1992)
16 Psyche (M)	0.087 ± 0.026	1.73	253.2 ± 4.0	2.0 ± 0.6	*Viateau* (2000), *Tedesco et al.* (1992)
20 Massalia (S)	0.0264 ± 0.0041	0.525	145.5 ± 9.3	3.26 ± 0.6	*Bange* (1998), *Tedesco et al.* (1992)
22 Kalliope (M)				2.5 ± 0.3	*Margot and Brown* (2001)
24 Themis (C)	0.289 ± 0.126	5.75			*Lopez Garcia et al.* (1997)
45 Eugenia (F)	0.030	0.60	214.6 ± 4.2	$1.2^{+0.6}_{-0.2}$	*Merline et al.* (1999)
87 Sylvia (P)	0.076	1.51 ± 0.15	260.94 ± 13.3	1.62 ± 0.3	J.-L. Margot (personal communication, 2001), *Tedesco et al.* (1992)
90 Antiope (C)			120.07 ± 4.0	1.3	*Weidenshilling et al.* (2001), *Tedesco et al.* (1992)
121 Hermione (C)	0.047 ± 0.008	0.93	209.0 ± 4.7	1.96 ± 0.34	*Viateau* (2000), *Tedesco et al.* (1992)
243 Ida (S)	0.00021	0.0042 ± 0.0006	31.4	2.6 ± 0.5	*Belton et al.* (1995)
253 Mathilde (C)	0.00052	0.0103 ± 0.0004	53.02	1.3 ± 0.2	*Yeomans et al.* (1997)
433 Eros (S)	0.0000336	0.00067 ± 0.00003	17.36 ± 1.2	2.67 ± 0.03	*Yeomans et al.* (2000)
704 Interamnia (F)	0.37 ± 0.17	7 ± 3	316.6 ± 5.2	4.4 ± 2.1	*Landgraf* (1992), *Tedesco et al.* (1992)
762 Pulcova (FC)			137.09 ± 3.2	1.8 ± 0.8	*Merline et al.* (2000), *Tedesco et al.* (1992)
804 Hispania (PC)	0.05 ± 0.04	0.995 ± 0.796	157.3 ± 5.3	4.9 ± 3.9	*Landgraf* (1992), *Tedesco et al.* (1992)
1999 KW4		$2.16 \pm 0.43 \times 10^{-7}$	1.2 ± 0.12	2.39 ± 0.9	J.-L. Margot (personal communication, 2001)
2000 DP107 (C)		$4.34^{+1.91}_{-0.56} \times 10^{-8}$	0.8 ± 0.15	$1.62^{+1.2}_{-0.9}$	J.-L. Margot (personal communication, 2001)
2000 UG11		$9.35^{+1.87}_{-3.74} \times 10^{-10}$	0.23 ± 0.03	$1.47^{+0.6}_{-1.3}$	J.-L. Margot (personal communication, 2001)

Current best estimates of mass and volume are shown in the top line of each asteroid listing along with the bulk density determination. For completeness, previous mass and volume determinations are also included.

tural weakness that break apart during impacts to form what become meteorites. Macroporosoity defines the internal structure of an asteroid. Those with low macroporosity are solid, coherent objects, while high macroporosities values indicate loosely consolidated objects that may be collections of rubble held together by gravity (see *Richardson et al.,* 2002).

1.2. Current Measurements of Asteroid Bulk Density

Spacecraft missions and advances in asteroid optical and radar observations have revolutionized our knowledge of asteroid bulk density. Shown in Table 1 and Fig. 1 is a summary of published mass and volume measurements. The methods of mass and volume determination are discussed in section 2.0, but a glance at Table 1 shows that before the 1990s bulk-density measurements were limited to a handful of the largest asteroids. In the past 10 years, the accuracy and breadth of these measurements has exploded and produced our first picture of the density structure of the asteroid belt. The largest three asteroids, Ceres, Pallas, and Vesta, have been studied for decades and have well-constrained values. These objects make up most of the mass of the asteroid belt. As shown in Fig. 1 in comparison with meteorite grain densities, these density values seem to make mineralogical sense. Because common geologic materials can vary by almost a factor of 4 in their grain density, asteroid bulk-density measurements need to be interpreted in terms of the object's mineralogy. The differentiated V-type asteroid 4 Vesta has a bulk density consistent with basaltic meteorites overlying an olivine mantle and metal-rich core. The primitive C-type asteroid 1 Ceres has a bulk density similar to primitive CI meteorites (for definitions of meteorite types see *McSween,* 1999). However, the smallest of these three asteroids is an order of magnitude more massive than the next well-characterized asteroids and these less-massive asteroids exhibit some intriguing trends. In general, S-type asteroids appear to have higher bulk densities than C-type asteroids, but the range in both groups is large. The M-type asteroid 16 Psyche, which is interpreted to have a mineralogy analogous to Fe-Ni meteorites, shows a bulk density in the range of hydrated clays. This indicates either very high porosity or a misidentification of the mineralogy. In the case of 16 Psyche, in addition to spectra and albedo consistent with metal, radar-albedo data strongly indicate a largely metallic surface.

2. THE DETERMINATION OF ASTEROID MASSES, VOLUMES, AND BULK DENSITIES

Though the number of asteroid density measurements has begun to increase rapidly in the last few years, still only a tiny fraction of the known asteroids have usable density measurements. A short history of the efforts to determine the masses of asteroids has been provided by *Hilton* (2002). Asteroid masses have been reliably determined from asteroid-asteroid or asteroid-spacecraft perturbations. That is, the mass

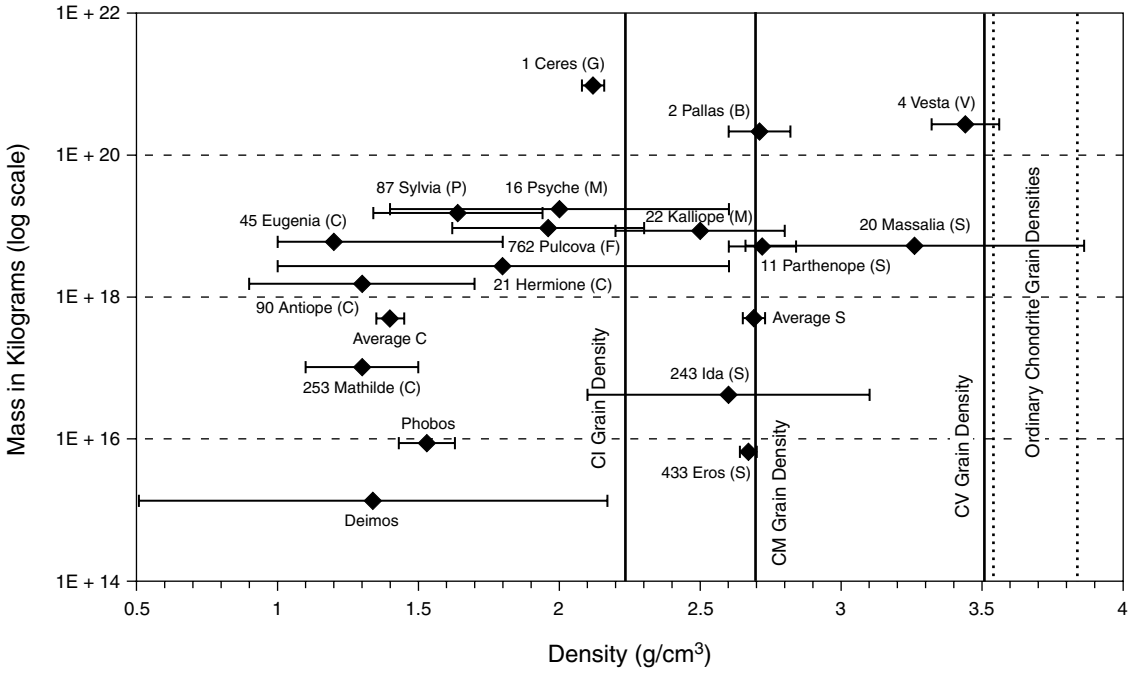

Fig. 1. Bulk densities of measured asteroids with the grain densities of common meteorites for comparison. Also included in the plot are the asteroidlike moons of Mars, Phobos and Deimos, as well as estimates for the average C- and S-type asteroids (*Standish,* 2001). Several asteroids in Table 1 with large error bars have been left off the plot for clarity.

of an asteroid is determined by observing the trajectory deviations of another asteroid, planet, or spacecraft after one or more close encounters. An asteroid's mass can also be determined by observing the motion of a satellite in orbit about the primary body since by Kepler's third law, the mass of the primary body can be determined if the orbital period and semimajor axis of the satellite are known. By far the most accurate method for determining an asteroid's mass, and even its mass distribution, is to track the motion of a spacecraft in orbit about it.

2.1. Asteroid Mass Determination Techniques

2.1.1. Asteroid mass determinations using their perturbations on neighboring spacecraft. The heliocentric change in velocity of an asteroid or spacecraft after a close asteroid approach is directly proportional to the mass of the perturbing asteroid and inversely proportional to both the close approach distance and relative velocity of the two bodies. For a perturbed spacecraft, the line-of-sight component of this velocity change is determined by observing the change in the Doppler tracking data during a close encounter. The close approach distance and relative velocity are determined from a spacecraft orbital solution that includes not only the spacecraft Doppler and range data but also the optical images of the asteroid before, during, and after the close flyby (see *Yeomans et al.,* 1997; *Yeomans et al.,* 1999). In practice, this solution provides not only the asteroid mass, close approach distance, and relative velocity but also several hundred other parameters associated with the solar radiation pressure, maneuvers and stochastic accelerations affecting the spacecraft, the surface landmark locations and spin characteristics associated with the asteroid, and the corrections required to the ephemerides of the spacecraft and asteroid. As a result of the Doppler and range tracking of the spacecraft and the optical asteroid landmark locations gathered by *NEAR Shoemaker* while in orbit about the asteroid Eros, this asteroid's gravity field, or mass distribution, was computed along with the total mass value (*Yeomans et al.,* 2000).

2.1.2. Mass determinations using the motions of their natural satellites. As of this writing, some nine asteroids have been identified as having satellites, and most of these objects were observed well enough that mass and density determinations were possible. Using *Galileo* imaging data of 243 Ida and its satellite Dactyl in August 1993, *Belton et al.* (1995) estimated the mass, volume, and bulk density for Ida. Groundbased adaptive optics at the Canada-France-Hawai'i Telescope (CFHT) were used to discover and observe satellites about asteroids 45 Eugenia (*Merline et al.,* 1999) and the transneptunian object 1998 WW31 (*Veillet et al.,* 2001), while Keck II adaptive optic images were used to discover and observe satellites about asteroids 87 Sylvia (J.-L. Margot, personal communication, 2001), 90 Antiope, and 762 Pulcova (*Merline et al.,* 2000). Goldstone and Arecibo radar imaging observations were used to identify and observe satellites about asteroids 1999 KW4 (*Benner et al.,* 2001), 2000 DP107 (*Margot et al.,* 2001), and 2000 UG11 (*Nolan et al.,* 2001). With the exception of 1998 WW31, at least preliminary values for the densities of all the double asteroids have been announced.

2.1.3. Mass determination using their perturbations on Mars. *Standish and Hellings* (1989) used the perturbations of asteroids on the motion of Mars to directly determine masses for the three largest asteroids. For perturbations with periods of 10 years or less, only Ceres, Pallas, and Vesta produce perturbative amplitudes of more than 50 m on the motion of Mars. The Mars observational dataset includes optical data back to the introduction of the impersonal micrometer in 1911 as well as more recent radio, lunar laser ranging, and radar data. However, it was primarily the *Viking* lander spacecraft data that allowed Mars range measurements to about 7 m (1976–1980) and 12 m (1980–1981) — well below the perturbative effects of these three minor planets. With additional observations of Mars, including the ranging and Doppler data from the *Mars Pathfinder* and *Mars Global Surveyor* spacecraft, this analysis has been updated recently (*Standish,* 2001) with the results being presented in Table 1. Although other, smaller asteroids had nonnegligible effects upon the orbit of Mars, a direct solution for their individual masses was not feasible because their perturbative effects were not substantially larger than the observational accuracy. However, Standish found it necessary to model these perturbative effects in the Mars ephemeris development effort. A mass was computed for each of a few hundred of the largest asteroids by using its estimated diameter and assuming a particular bulk density based upon its spectral class. By accumulating the perturbations of each spectral class together, it was possible to solve for the mean bulk density for the spectral class as a whole. For a recent solution completed after the release of JPL Development Ephemeris number 405 (DE405), the mean bulk densities were computed to be 1.4 (±0.05), 2.69 (±0.04), and 4.7 (±0.5) for the C-, S-, and M-asteroid spectral types respectively (E. M. Standish, personal communication, 2001).

2.1.4. Mass determinations from asteroid-asteroid interactions. The largest number of asteroid masses has been computed using the observed motions of asteroids that have interacted with other asteroids either one or more times. The more recent results are given in Table 1. Relatively precise mass determinations have been computed in this fashion for the three largest asteroids, 1 Ceres, 2 Pallas, and 4 Vesta (see Table 1). *Hilton* (1999) concluded that attempts to compute the mass of Ceres or Pallas by itself would lead to errors since the mass determination for either one was dependent upon the other's assumed mass. To avoid what he considered a computational degeneracy, he simultaneously solved for the masses of Ceres, Pallas, and Vesta. However, the masses he obtained for Ceres and Pallas are discordant with other solutions, including recent ones by *Michalak* (2000), *Goffin* (2001), and *Standish* (2001), where simultaneous mass solutions were also determined for more than one asteroid. *Goffin* (2001) pointed out that his results for the mass of Pallas were relatively insensitive to the assumed mass of Ceres. While

the masses of Vesta determined by *Standish* (2001), *Michalak* (2000), *Goffin* (1991), *Schubart and Matson* (1979), and even the very first reliable asteroid mass determination by *Hertz* (1966) are all consistent, the result by *Hilton* (1999) is again discordant with the others. In Table 1, we have selected the Ceres, Pallas, and Vesta masses determined by *Standish* (2001) for the given bulk-density determinations.

2.2. Volume Estimates

Asteroid volume estimates are most often made using an effective radius determined by the Infrared Astronomical Satellite (IRAS) Minor Planet Survey (*Tedesco et al.,* 1992). Because of corrections and refinements to the data-reduction process, care must be taken to use the 1992 publication rather than the earlier results presented by *Tedesco* (1989). For a select few asteroids, their shapes and hence their volumes can be determined by occultation techniques. For the bulk density of 2 Pallas displayed in Table 1, an occultation derived volume has been employed (*Dunham et al.,* 1990). Volume estimates based upon Hubble Space Telescope and groundbased adaptive optics techniques have been used for 1 Ceres (*Drummond et al.,* 1998), 4 Vesta (*Thomas et al.,* 1997), 45 Eugenia (*Merline et al.,* 1999), and 87 Sylvia (J.-L. Margot, personal communication, 2001). Radar images of double asteroids 1999 KW4, 2000 DP107, and 2000 UG11 have been taken and J.-L. Margot (personal communication, 2001) has provided preliminary estimates for their masses, radii, and bulk densities. Spacecraft imaging data were used to determine the shapes and volumes for 243 Ida (*Belton et al.,* 1995) and 253 Mathilde (*Veverka et al.,* 1997). For asteroid Ida, complete (but distant) imaging coverage from the *Galileo* spacecraft allowed a volume determination to the 12% level. Because of Mathilde's 17.4-d rotation period, complete imaging coverage of the surface was not achieved during the *NEAR Shoemaker* spacecraft flyby, allowing only a 15% volume determination. On the other hand, the volume for 433 Eros was determined to the few percent accuracy level using the imaging and laser rangefinder data onboard the orbiting *NEAR Shoemaker* spacecraft (*Veverka et al.,* 2000; *Yeomans et al.,* 2000; *Zuber et al.,* 2000). In Table 1, the effective diameters given for Ceres, Pallas, and Vesta were determined from the volume estimates computed using their major and minor figure axes.

2.3. Bulk Density Determinations

In Table 1, the best mass and volume determinations together with their respective uncertainties have been employed to determine the given bulk densities and their associated uncertainties. For asteroids for which multiple estimates are provided for either the mass or volume, the best estimate listed in each case has been used to compute the given bulk density. The mass estimate for 20 Massalia was taken from *Bange* (1998) assuming the mass of Vesta is that given by *Standish* (2001). A few data gaps appear in Table 1 because some values were not available in the published literature. For example, only the bulk densities for 90 Antiope and 762 Pulcova have been published, so the corresponding mass estimates are not available and we could not locate a reliable effective diameter for 24 Themis.

3. CONSTRAINTS ON ASTEROIDS FROM METEORITE DATA

3.1. Selection Effects and Asteroid Analogs

To what degree can we use meteorites measured in our laboratory to put constraints on the density and structure of asteroids? There is little doubt that meteorites do sample the asteroid belt. There is somewhat less certainty that the meteorites are a complete or representative sample of the belt (cf. *Sears,* 1998; *Meibom and Clark,* 1999). Selection effects in ejection from the parent asteroid, transportation to Earth, and atmospheric entry certainly play a major role in the population of meteorites reaching our collections.

The overwhelming majority of meteorites (some 75% of those seen to fall, ~85% of those collected from dry deserts, and >90% of those found in Antarctica) are stony meteorites of the class known as "ordinary chondrites" (*Grady,* 2000). A comparison of observed fireball rates with meteorite recoveries in desert areas (*Bland et al.,* 1998) indicates that the total number of objects hitting the Earth's atmosphere is within a factor of 2, at most, of the number of similar-sized objects hitting the ground. This still allows the possibility that the vast majority of weak meteorites, like the most friable carbonaceous types (e.g., CIs) could be broken up and lost in the atmosphere. But such meteorites are so rare in our collections that even if 99% of them were lost in Earth's atmosphere, they would still only have an abundance in space comparable to ordinary chondrites. That would be consistent with the fireball statistics. Even in that event, however, a significant fraction if not the absolute majority of meteorites falling today would still be ordinary chondrites. Thus, at a minimum, at least half the meteoroids arriving at Earth today are ordinary chondrites. (It is important to note that samples of the most abundant types of carbonaceous chondrites, the CV and CO classes, are essentially as dense and as strong as ordinary chondrites; passage through the atmosphere should not strongly discriminate against them.)

Another kind of selection effect is temporal. We know with some certainty what sort of meteorites have hit Earth in historic times and we know, with a bit more uncertainty, that similar distributions of meteorites have accumulated in Antarctica over the past 10,000 to 100,000 yr. Attempts to "mine" meteorites from beds of various geologic ages (or from the Moon) have proved difficult so far, and in any event, the populations do not show any significant changes in the kinds of materials recovered. One cannot rule out the possibility that the flux of meteorites hitting Earth today represents a chance sampling from a small number of sources. Different types of meteorites may have been prevalent on Earth 1 b.y. ago. More to the point, different types of

meteorites, unsampled by anything hitting Earth now, may be prevalent in the asteroid belt today. Indeed, there is a range of spectra among the S-type asteroids that show relative abundances of pyroxene and olivine with no direct analogs in our collections (*Gaffey et al.,* 1993). Given that possibility, how reasonable is it to use meteorite physical characteristics to set limits on asteroidal structure?

There are, however, three arguments to suggest that meteorites in our collections today are a reasonable place to start to predict the density and structure of material making up the asteroids. First, it is noteworthy that the spectra even of the S types not sampled in our collections remain essentially mixtures of these same minerals, pyroxene and olivine, albeit in differing proportions with differing FeO contents. Furthermore, the abundances of the rock-forming elements seen in solar spectra are not significantly different from the abundances seen in ordinary chondrite meteorites. There are only so many ways that these elements can be formed into minerals, and it is unlikely that the vast majority of material in the asteroid belt should be anything but these expected minerals (olivine, pyroxene, and plagioclase). Finally, there are physical limits to the porosity state in which coherent rocks can be found; the same evidence that suggests a body like asteroid Eros can maintain geological coherence also places limits on the microstructure of the rock that transmits that coherence. In any event, it is clearly better to start with data of material we know comes from the asteroid belt than to speculate, without data, about what may or may not be present there.

3.2. Measurement of Meteorite Density and Porosity

Measurement of meteorite density is hampered by two concerns: the risk of contamination and the (*a priori* unknown) effect of microporosity. The traditional methods for measuring the density of rocks (and other irregularly shaped objects) are based on the method of Archimedes: immersing the sample in a fluid and measuring either the sample's displacement of a measured volume of fluid or the relative weight of the sample in the fluid compared to its weight in air. But for meteorites, the problem of contamination is serious: Water can alter or remove indigenous salts and other soluble minerals in the meteorite and promote the oxidation of metallic Fe often present in tiny grains that are especially vulnerable to weathering. Organic fluids such as CCl_4, which have also been used, carry with them their own possible organic contaminants.

Even without these contamination worries, however, a second issue is the question of porosity. One must assume these samples could have significant porosity; indeed, a goal of our measurements is to determine that porosity, which is the ratio of the bulk volume (given by the outer shape of the sample) to the grain volume (that of the minerals within the rock, not including voids, microcracks, and other flaws in the rock fabric). But any liquid may enter into the pore spaces to some unknown extent; thus the volume measured will be neither the bulk volume nor the grain volume.

To get around these issues, gases are commonly used as the Archimedean fluid in grain-density measurements. In a typical pycnometer, the sample is placed in a chamber of known volume and flushed with He at a known pressure. A second chamber, also of known volume, contains helium at a higher (known) pressure. The two chambers are connected and pressures equalized; the final pressure indicates how much of the given chamber volumes is taken up by the grain volume of the sample. Helium is known to be nonreactive, and at least in ordinary chondrites it can be expected to penetrate quickly into all pore spaces and voids. (An examination of meteorite thin sections shows that most porosity comes as a dense network of microcracks, generally <10 μm wide. Helium would only have to diffuse a distance of <100 μm from these cracks, through fine-grained material, to reach any voids not connected by these cracks.)

Consolmagno and Britt (1998) adapted an unusually large pycnometer to measure large (up to several kilograms) meteorite specimens. To measure bulk densities, they developed a method using 40-μm glass spheres as the Archimedean fluid; the spheres are nonreactive, are easy to see and brush off the samples after measuring, and clearly do not penetrate into the cracks and pores. From these data, porosities could be measured directly on dozens of meteorites. This work has been supplemented by new data from *Flynn et al.* (1999) and *Wilkison and Robinson* (2000), who measured additional grain and bulk densities respectively.

3.3. Results of These Measurements: Porosity and Density of the Meteorite Classes

Along with their data analysis, *Consolmagno et al.* (1998) incorporated a detailed literature search of meteorite densities and porosities (most notably a large database collected by *Terho et al.,* 1993) into the study of general trends in ordinary chondrites. In all, more than 160 meteorite porosities and nearly 400 density measurements were analyzed. They concluded that weathering of meteorite falls reduces most ordinary chondrite porosities as a function of exposure time in the terrestrial atmosphere.

Consolmagno et al. (1998) noted that one could assume a grain density for each meteorite chemical type (H, L, or LL) since the grain density should be only a function of composition, which is specified by the type classification. They suggested that bulk density is not significantly changed due to mild weathering, since the filling of pore spaces by weathering product will not change the outer shape of the meteorite and the weathering-related mass flux (mostly terrestrial O reacting with meteoritic Fe) will amount to only a few percent of the total meteorite mass. Thus, they conclude that a model preweathering porosity can be estimated for each meteorite by comparing measured bulk densities against theoretical grain densities. When applied to the ordinary chondrites for which bulk densities have been measured (presently numbering ~300), they find the distribution of model porosities shows no dependence on meteorite type or metamorphic grade. All meteorite porosities so estimated

fall into a bell-shaped distribution centered on 11% porosity with a 1σ spread of ±5%. This distribution is shown in Fig. 2. The average model grain density, bulk density, and model porosity for each subtype of ordinary chondrite are shown in Table 2.

Consolmagno et al. (1999) explain this distribution by noting the visible evidence of porosity in meteorite thin sections. Virtually all the porosity of an ordinary chondrite can be attributed to a network of cracks, roughly 10 μm wide, that have been emplaced onto the meteorite fabric (presumably by impacts) after the meteorite was accreted and lithified. In find meteorites, these cracks are filled with weathering product (the microprobe detects Fe and Cl, but no Ni) and in some older falls, these cracks can be seen to be half-filled with weathering product, extending out from Fe-Ni grains; in the freshest falls, the cracks are empty. This is in line with the hypothesis that weathering in ordinary chondrites primarily fills porosity with oxides (cf. *Bland et al.,* 1998) and the presence of the weathering product also confirms that these cracks are indeed present in the meteorite and not an artifact of the thin sectioning.

The situation for C-type meteorites is more complex. These meteorites arrive on Earth already quite oxidized, and so it is more difficult to determine the extent to which terrestrial weathering has filled pore spaces. These meteorites are also much rarer than ordinary chondrites, and tend to come in much smaller samples, thus making the collection of their density and porosity data much more difficult. Only a handful of these meteorites have had their porosities and densities reported (cf. *Britt and Consolmagno,* 2000). The range of porosities is much higher — from zero to over 30% for various samples of the CI, Orgueil, and from near-zero (Vigarano) to 25% (Allende) for two different CVs.

The bulk densities of C-type meteorites, however, fit into two ranges: CI and CM meteorites, characterized by significant water content and low Fe, have bulk densities around 2 g/cm^3, while most dry (CO and CV) or more Fe-rich (CR) carbonaceous meteorites have densities between 2.9 and 3.5 g/cm^3, essentially indistinguishable from the bulk densities of ordinary chondrites.

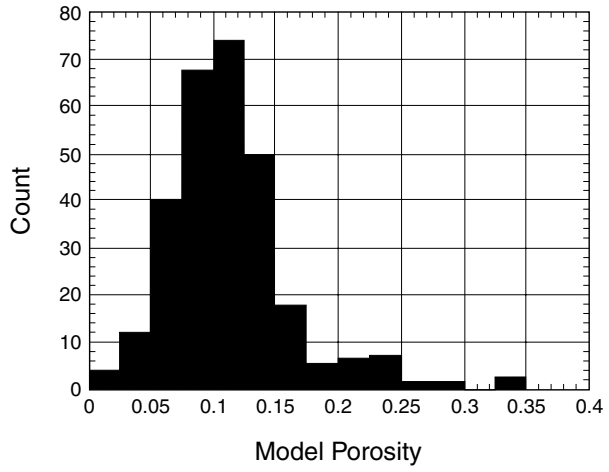

Fig. 2. Ordinary chondrite model porosities.

TABLE 2. Average densities for meteorite types.

Meteorite Type	Grain Density	Average Bulk Density	Average Porosity
H ordinary chondrites	3.84	3.40	11.5%
L ordinary chondrites	3.75	3.34	10.8%
LL ordinary chondrites	3.56	3.19	10.4%
Achondrites	3.20	2.97	7.0%
CI carbonaceous chondrites	2.27	2.12	11%
CM carbonaceous chondrites	2.71	2.21	12%
CR carbonaceous chondrites	3.11	3.15	6%
CV carbonaceous chondrites	3.51	3.10	11%
CO carbonaceous chondrites	3.69	3.11	16%

4. ASTEROID POROSITY

Given knowledge of meteorite porosity and bulk density, and the growing database of asteroid bulk-density measurements, we can start to estimate the porosity of asteroids and assess their internal structure. The starting points are the three pieces of data we have about an individual asteroid: (1) the bulk density, (2) the reflectance spectrum that provides a meteoritic compositional analog, and (3) the grain density and average porosity of the analog meteorite. Since the meteorite grain density gives the density of the asteroid if it was a completely solid object, the deviation of the asteroid's bulk density from this provides an estimate for the bulk porosity of the asteroid. This is essentially scaling the raw bulk-density data by the asteroid's meteorite analog. The assumption that the pore space is empty establishes a lower bound on the porosity of the asteroid. Since empty space has no density itself, this is the minimum amount of low-density volume needed to reconcile the observed bulk density with the grain density of its mineralogy. If the pore spaces were filled with some material such as water-ice, the amount of pore space required to explain the low bulk density of the object increases dramatically. In the case of low-density objects like 243 Mathilde or 90 Antiope with bulk densities of 1.3 g/cm^3, their bulk densities are not significantly higher than water-ice (at 0.97 g/cm^3) and would require unrealistically huge (i.e., >75 vol%) components of water-ice to account for their low densities given the grain density of their meteorite analogs (*Britt and Consolmagno,* 2000).

The estimated bulk porosities of the asteroids in Fig. 1 are shown in Fig. 3. This figure highlights the emerging structure of the asteroid belt. First, low-porosity objects are relatively rare. Aside from the three largest asteroids, the only other asteroid with an estimated porosity of <15% is 20 Massalia. Most asteroids have significant porosity. There is a cluster of objects around 30% porosity and a scattering of objects on the high end all the way out to 16 Psyche and 22 Kalliope with total porosities of more than 70%.

These data reflect the bulk porosity, which is the sum of all the asteroid's porosity, including the microporosity found

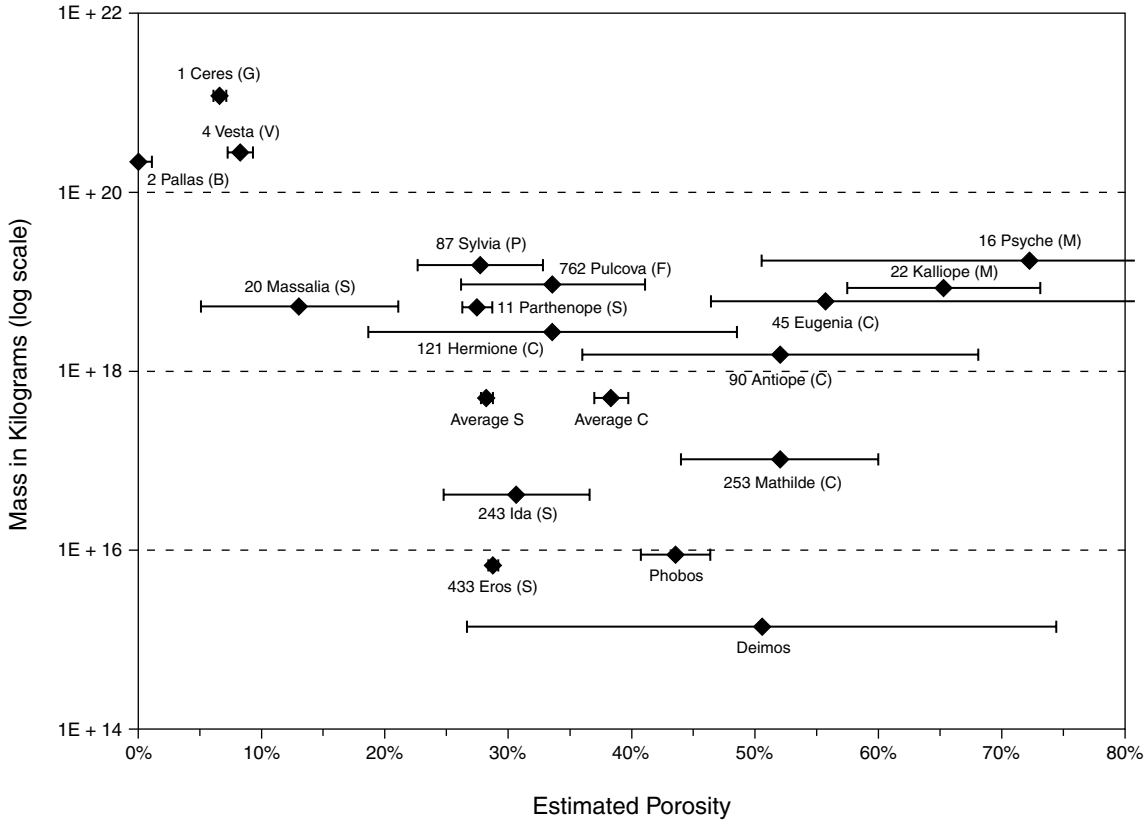

Fig. 3. Estimated porosity of measured asteroids. The bulk density of the asteroid is scaled by the grain density of its best meteoritic spectral analog to provide an estimate of the asteroid's total porosity. This includes the small-scale microporosity common in meteorites and the large-scale macroporosity that can affect the asteroid's structure.

in meteorites as well as the large-scale macroporosity. Microporosity probably does not seriously affect the parent asteroid's internal strength since this level of small-scale porosity survives in meteorites that have survived ejection, transportation, and delivery to Earth. For insight into the asteroid's internal structure, we need to extract an estimate of the asteroid's macroporosity from its bulk porosity. Subtracting the average meteorite analog microporosity from the bulk porosity of an asteroid provides a rough estimate of the asteroid's large-scale macroporosity. Note that this estimate requires two assumptions: first, that we know the asteroid's meteorite analog and, second, that the meteorites delivered to Earth are a representative sample of that material.

Shown in Fig. 4 are the estimated macroporosities for these asteroids. These data appear to divide into three rough groups. The first group includes the large asteroids 1 Ceres, 2 Pallas, and 4 Vesta, as well as the somewhat smaller 20 Massalia. Their bulk densities are very close to the grain densities of their analog meteorites, indicating essentially zero macroporosity. These asteroids are probably strong, coherent objects that have not been disrupted throughout solar-system history. It is interesting that all three asteroids with diameters >500 km fall in the zero-macroporosity group and only one other smaller asteroid has low macroporosity. This probably indicates a very strong size selection process within the asteroid belt for survival as a coherent object and perhaps the relative rarity of coherent smaller asteroids.

The second group includes the S asteroids 433 Eros and 243 Ida as well as 762 Pulcova and 121 Hermione. These asteroids have between 15% and 25% macroporosity, indicating that they have been extensively fractured. Spacecraft images of both 433 Eros and 243 Ida show numerous morphological indications of pervasive fracturing (*Belton et al.,* 1995; *Veverka et al.,* 1997; *Veverka et al.,* 2000). However, this fracturing was probably not extensive enough to disrupt the object and asteroids with less than approximately 25% macroporosity probably have some measure of coherent strength. In terrestrial geology, well-sorted sedimentary rocks can have up to 30% porosity and still be coherent. However, porosities larger than ~30% usually indicate loose rubble or soils.

The third group are those with greater than 30% macroporosity. These objects, some of which have more empty space than solid material, are probably pervasively fractured and may have been disrupted and reassembled by mutual gravity. Asteroid 16 Psyche is likely the most porous object observed so far. Its reflectance spectra and radar albedo strongly indicate a metallic surface composition. Assuming

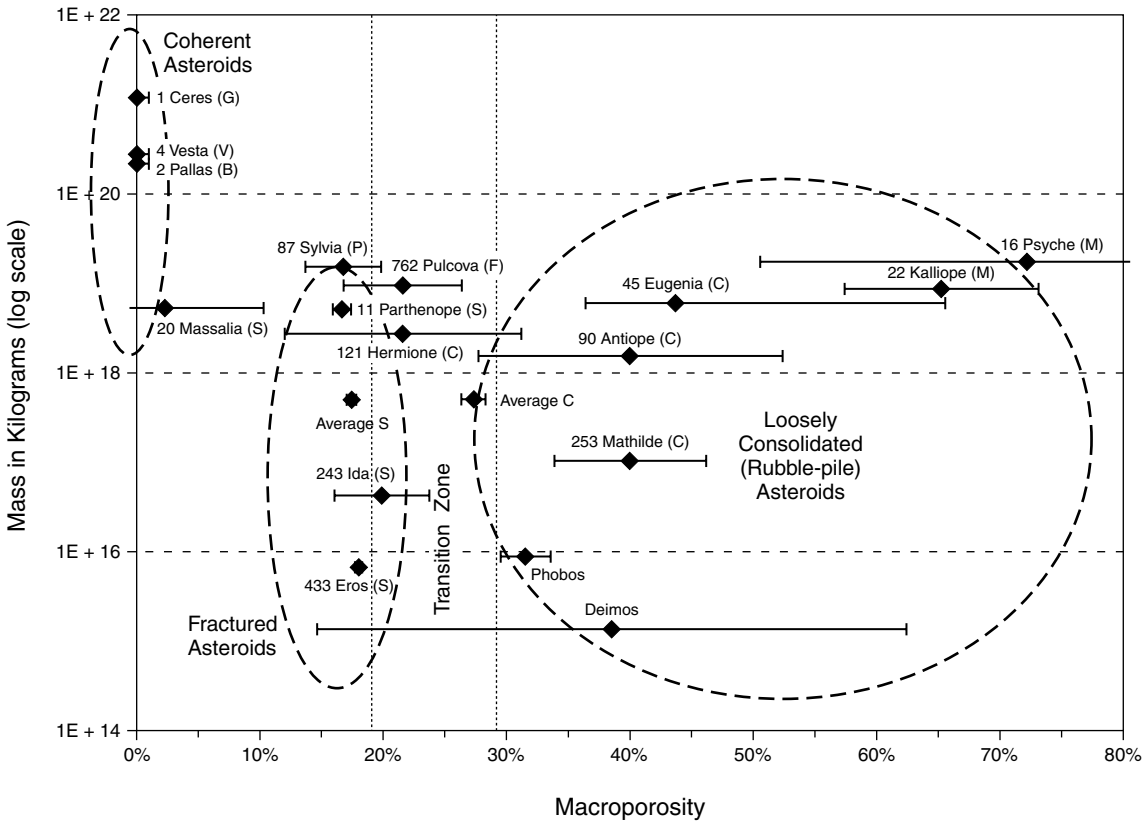

Fig. 4. Asteroid macroporosity estimated by subtracting the average porosity of asteroid's meteorite analogue from the bulk porosity shown in Fig. 3. Since microporosity probably does not seriously effect the structural integrity of asteroids, this is a direct estimate of the large-scale fractures and voids that determine the asteroid's internal structure.

a iron meteorite grain density of 7.4 g/cm^3, this would require a bulk porosity of 75%. Iron meteorites have essentially zero microporosity, so the bulk porosity in this case likely equals the macroporosity suggesting a pervasively disrupted object that has been loosely reassembled and held together by mutual gravitation.

It is also interesting that each of these three groups contain representatives of a range of asteroid spectral types. The group coherent asteroids contains of two primitive spectral types, the C-type 1 Ceres and the B-type 2 Pallas that have mineralogies of low-temperature condensates, organics, and hydrated minerals. But this low-porosity group also contains the differentiated V-type 4 Vesta with a basaltic crust and the high-temperature, mafic silicate-rich S-type 20 Massalia, both of which have strikingly different mineralogies from the first pair.

In general, the dark, primitive asteroids seem to be more prevalent in the "rubble-pile" group, while the high-albedo, higher-temperature S-type asteroids seem to be more common in the "fractured" group. The average S-type bulk density determined by E. M. Standish (personal communication, 2001) falls in the fractured group while the average C-type bulk density is closer to the rubble-pile group. This may indicate that primitive asteroids are fundamentally weaker and more likely to be loosely consolidated, while the metamorphic and igneous asteroids tend to be stronger and more likely to be coherent. However, there are glaring exceptions in each group, such as the low-porosity P-type 87 Sylvia. Fundamentally, what these data tell us is that the collisional disruption history of the asteroid belt is complex and probably stochastic, that mineralogy affects but does not control macroporosity, and that most asteroids have and retain significant porosity.

5. ASTEROID POROSITY AND IMPACT PHYSICS

The response of an asteroid to a collision event is determined by the manner in which stress waves generated by the impact are propagated and attenuated throughout the body. Stress-wave propagation is, in turn, governed by the mechanical properties and shape of an asteroid and its internal structure, i.e., the size and spatial distribution of fractures and pore spaces. Similarly, the occurrence of an impact can drastically alter the internal structure of an asteroid, through the creation of additional fractures and large-scale pore spaces or the reduction of porosity through compaction. It is important to understand these coupled processes

because they are major drivers in the collisional evolution of asteroids.

This section considers the interplay between the porosity of an asteroid and the outcomes of collision events. This is a complex and relatively immature field, with important and interesting problems yet to be studied. This section highlights some of the important issues for collisions involving porous bodies.

5.1. Effect of Porosity on Collisions

The principal effect of target porosity on collisional outcomes is to attenuate the stress wave generated in an impact. As a strong shock propagates though a porous target, energy is expended (in PdV work) to collapse the pore spaces, which contributes to irreversible heating of the target. In addition, pore spaces, depending on their size scale, disperse or scatter the shockwave front. Both of these mechanisms serve to make porous materials much better attenuators of shock pressure than nonporous materials.

The dissipative nature of porous materials has been observed in experimental simulations of collisional fragmentation (*Holsapple et al.,* 2002). For example, *Stewart and Ahrens* (1999) performed experiments with plaster targets having a porosity of 65%. The tensile strength of the plaster was about a factor of 10 below that of competent basalt. Even so, the targets behaved as if they were quite strong and the projectile energy per unit target mass for catastrophic disruption was very close to that measured for basalt. Apparently, the shock attenuation in the porous target was large enough to offset the low tensile strength. This, along with similar results for other materials (e.g., *Nakamura et al.,* 1992; *Love et al.,* 1993) suggest that weak porous asteroids could be quite resistant to collisional disruption. This is discussed in more detail below.

Efficient shock dissipation is also evident in craters formed in porous materials. For example, the large craters on the porous asteroid Mathilde are packed closely together with little evidence of shock-induced disturbance of adjacent craters (*Veverka et al.,* 1997; *Chapman et al.,* 1999). This effect has been reproduced in laboratory experiments in which impact craters were formed in highly porous materials (*Housen et al.,* 1999). The experiments were performed on a centrifuge in order to satisfy the similarity requirements needed to replicate the formation of large craters on asteroids. Figure 5 shows an example of two craters formed in a material with ~60% porosity. The experiments demonstrated that craters form in close proximity (rims nearly touching), with no damaging effects on earlier craters. Evidently, shocks damp out extremely quickly in the presence of high porosity.

Numerical simulations of collisions have provided another interesting insight into the propagation of shocks in porous asteroids. *Asphaug et al.* (1998) reported on smoothed particle hydrodynamic (SPH) simulations of an impact into a model asteroid represented by a collection of nonporous boulders. The size scale of the pores was comparable to the size of the impactor. They too found that the shock was effectively dissipated due to the energy used in pore collapse. In addition, scattering of the shock due to the large-scale heterogeneity of the target caused the impact energy to be deposited in a localized volume, resulting in high velocities of ejected debris. This could have significant implications for disruption and ejecta retention on rubble pile asteroids composed of fragments that are comparable to, or larger than, an impacting body.

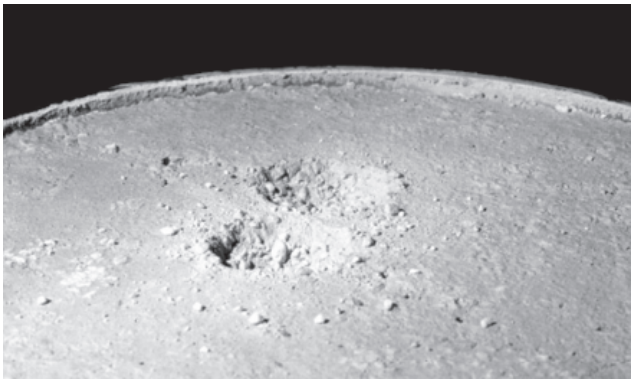

Fig. 5. Two craters formed sequentially in a target having initial porosity of 60%. Images of the first crater (furthest from camera) before and after the second impact showed no noticeable damage caused by the second impact, even though the crater rims were nearly touching. The porous material efficiently damps the shock pressure.

5.2. Effect of Collisions on Asteroid Porosity

Because fractures and porosity can have such a dramatic effect on the collisional response of asteroids, it is important to also consider how collisions affect the internal structure of asteroids. Numerous laboratory and numerical studies have addressed this problem (*Holsapple et al.,* 2002; *Asphaug et al.,* 2002).

It is generally accepted that impacts below the threshold energy for catastrophic disruption leave a body highly fractured, but mostly intact. Eros is probably an example of such a fractured shard (*Britt and Consolmagno,* 2000; *Veverka et al.,* 2000; *Wilkison and Robinson,* 2000). Impact-generated fractures provide for modest increases in porosity. Much larger increases are probably attained in the energetic collisions that shatter a body and temporarily disperse the fragments, which then reaccumulate into a rubble pile. Using terrestrial soils and rocky debris as an analogy, it is reasonable to expect catastrophic collisions to produce rubble pile structures having macroporosity in the range of 30–50% (e.g., *Lambe and Whitman,* 1969; *Britt and Consolmagno,* 2000).

Interestingly, an analogy to rubble-pile formation can be found in the literature of explosive field cratering. When the depth of burial of an explosive charge is less than criti-

cal in value, a crater is formed by excavation and ejection of material in a manner similar to the formation of most impact craters. On the other hand, explosives buried slightly deeper than the critical depth launch debris nearly vertically. These ejected fragments do not "escape" the crater, but instead fall back to the surface with little horizontal translation. The jumbled material may bulk considerably, leaving a mound instead of a crater.

Figure 6 shows the result of a deep explosion in competent basalt. Ejected rock fragments rose to a height of some 30 m and reaccumulated into a rubble pile with a diameter of 46 m and a height of 8 m. The bulk porosity increased from an initial value of ~8% to a final value of ~30%. A trench dug through the mound showed fragments ranging from very small sizes up to more than 1 m, with significant pore space over a corresponding range in size scale. The largest blocks in the mound had dimensions comparable to the spacing of fractures in the preshot material, suggesting that block size was controlled by the spacing of *in situ* fractures. The same mechanism probably applies to rubble-pile formation of asteroids. That is, the size distribution of fragments that end up in a rubble pile from a catastrophic collision will depend on the varied fracture systems generated in previous noncatastrophic impacts.

In contrast to the above mechanism, an asteroid that already has high porosity, either as a remnant of accretion processes or from rubble-pile formation, can experience a net reduction in bulk porosity during collisions. Shocks in highly porous asteroids act as compaction waves closing pore spaces as they damp out in the body (*Menikoff,* 2001).

In granular geological materials, compaction occurs in two ways. First, at low pressures, grains can slide past one another into a more compact configuration. This occurs when the pressure is sufficient to cause elastic deformation in the grains, overcome frictional forces at grain boundaries, or break the intergranular bonds in cemented aggregates. This simple geometrical rearrangement is possible as long as the bulk density is below a threshold value, which is referred to in the soil-mechanics community as the maximum relative density. (In soil mechanics, the term "maximum relative density" refers to the highest density that can naturally be attained without fracturing the constituent grains. Tapping, vibration, and pluviation are typically used to attain the maximum-density state for soils.) Therefore, as long as the constituent grains or rubble fragments of an asteroid are not in their maximum-density configuration, a reduction in porosity can occur at relatively low pressures (the magnitude of the pressure depends on the shape and the mechanical and frictional properties of the grains). This provides an opportunity for subcatastrophic collisions to reduce the bulk porosity of a rubble pile by seismically shaking the fragments into a more compact configuration.

Fig. 6. Side view of the rubble pile produced in a buried nuclear explosion (codename SULKY) in competent basalt. The mound is approximately 46 m in diameter and 8 m high.

The second mechanism that reduces porosity in granular materials occurs when the applied pressure is large enough to fracture the grains, thereby allowing additional movement and better packing. For silicate soils, grain fracture initiates when the pressure exceeds ~10 MPa, although significant compaction requires more than ~100 MPa (*Hagerty et al.,* 1993; *Yamamuro et al.,* 1996). During impacts into dry sand at a few kilometers per second, these pressures are reached only in a localized region near the impact point. As a result, the volume of compacted material produced by impacts in dry sand is very small compared to the crater volume. This is true even for sands that have been intentionally fluffed up to increase their porosity. Viewing a rocky rubble-pile asteroid as a collection of large sand grains, one might conclude that subcatastrophic collisions would not be very efficient at compacting the rubble by this mechanism.

However, it is important to note that while silicate grains require high pressures for fracture, the "grains" in an asteroid rubble pile could range from typical mineral grains up to fragments or aggregates of considerable size. The pressure required to fracture large fragments is probably much smaller than 10 MPa. For example, chunks of rock tend to weaken with increasing size, roughly as $L^{-1/2}$, where L is the linear size of the rock sample (*Lundborg,* 1967). Moreover, in a C-type rubble-pile asteroid, the fragments might be very weak, with strengths comparable to those of carbonaceous meteorites. As such, the crushing strength of the "grains" might be small enough that shock compaction could be quite efficient.

An example of shock compaction was reported by *Housen et al.* (1999) and *Housen and Voss* (2001). They performed impact-cratering experiments in silicate materials and varied the porosity from 35% to 70%. Compaction, as opposed to excavation, was found to be the dominant mechanism of crater formation when the target porosity was greater than ~40%. When the porosity exceeded ~55%, only a small part of the material originally within the crater was excavated and emplaced into an external ejecta deposit. That is, most of the crater volume was formed by permanent compression of the target material. A consequence of such compaction events is that the target volume is reduced, thereby increasing its bulk density. Applying this result to Mathilde, the five largest craters on Mathilde would have increased its bulk density by ~20%. This value would be even larger

if additional big craters are discovered on the as-yet-unobserved hemisphere. Hence, if Mathilde's large crater population is typical of initially porous asteroids, compaction cratering could be an important mechanism for reduction of porosity.

It should be emphasized that porosity may not be the most important property that determines whether collisions will compact an asteroid. For example, it is likely that two asteroids with the same porosity, one metallic and one carbonaceous, would respond differently in collisions. A more relevant property might be a measure of the compaction strength, since this determines the volume of material crushed by the shock. One of the outstanding problems in studies of asteroid collisions is to determine the fundamental mechanical and physical properties that determine collisional outcomes.

5.3. Collisional Lifetimes of Porous Asteroids

The collisional lifetime of an asteroid is determined by the size distribution and flux of impacting bodies, the relative velocity of a collision, and the threshold size of the impactor capable of shattering or dispersing the body. The size distribution, flux, and relative velocity of objects in the main belt have been determined with reasonable certainty (e.g., *Farinella and Davis,* 1994; *Bottke et al.,* 1994). On the other hand, the impactor conditions required to shatter or disperse an asteroid are much more uncertain (*Holsapple et al.,* 2002). Numerical simulations can provide some guidance, but the material models used in hydrocodes are not yet sufficiently robust to predict collisional outcomes with certainty. This is especially true when considering porous asteroids; none of the numerical models in use at present have incorporated equations of state or constitutive models for porous materials. This is partially due to the fact that porous asteroids have only recently become of interest, but can also be attributed to the fact that the mechanical behavior of porous materials is not fully understood.

Laboratory experiments can provide some insights. However, it is very difficult to perform collision experiments under conditions that are directly applicable to collisions of kilometer-scale asteroids. By necessity, these studies must be conducted at small scales, where the effects of gravity are negligible compared to the cohesive strength of the target. As a result, the conditions required to shatter a small model asteroid are quite different from those required for a large object (*Holsapple,* 1993; *Housen and Holsapple,* 1999). While the scaling issues are understood to some degree for brittle nonporous materials (like rock), highly porous targets are completely different. Fundamental questions remain about which material properties are important and how porous asteroids fail during collisions. With these caveats in mind, we consider the current state of knowledge concerning catastrophic collisions of porous asteroids and how their collisional lifetimes might differ from those of nonporous bodies.

Asphaug et al. (1998) used their SPH code to model an impact into nonporous and porous models of Castalia. The impactor they considered was able to fracture the nonporous model significantly, but only ~10% of the mass of fragments were able to escape. An identical impact into a weak porous model produced more localized damage, but accelerated nearly half of the excavated fragments to escape velocity. This suggests porous weak asteroids could have shorter collisional lifetimes than their nonporous counterparts. But it is important to note that these simulations considered porosity only at scales comparable to the impactor size. Different results might be obtained for a model target consisting of porous boulders.

A somewhat different result is indicated by laboratory experiments. *Ryan et al.* (1999) impacted porous and nonporous ice targets with various projectiles and found that, even though the porous targets were mechanically weaker than their solid counterparts, the porous targets required about the same kinetic energy per unit target mass, Q^*, for shattering. Evidently, the shock dissipation in the porous targets was enough to offset their lower strength. *Stewart and Ahrens* (1999) reached a similar conclusion for targets made of plaster. *Love et al.* (1993) impacted sintered glass bead targets having various porosities and strengths. Based on a small number of experiments, *Love et al.* presented the following tentative relationship for Q^*

$$Q^* \propto S^{0.45} (1 - n)^{-3.6} \quad (1)$$

where S is the strength and n is the bulk porosity of the target. This is in qualitative agreement with the other experimental results in that low target strength tends to offset high porosity. For a constant target strength, this relation implies that Q^* for an asteroid with 60% porosity would be ~8× larger than for a body with 30% porosity.

The dependence of collisional lifetime on bulk porosity can be estimated as follows: By definition, $Q^* = 0.5a^{*3}\delta U^2/(\rho R^3)$, where a^* is the threshold impactor radius required for shattering, ρ is the bulk density of the asteroid, δ is the impactor density, U is the impact velocity, and R is the asteroid radius. For a given impactor density, impact velocity, and asteroid radius, $Q^* \propto a^{*3}/\rho$. Additionally, the bulk density is related to the porosity n and the grain density ρ_g by $\rho = (1 - n)\rho_g$. Substituting these expressions into equation (1) shows that $a^* \propto (1 - n)^{-0.87}$. *Farinella and Davis* (1994) estimate that the flux of impacting bodies in the main belt is proportional to the –2.5 power of the impactor radius. The collisional lifetime against shattering (which is inversely proportional to the flux) is therefore proportional to $(1 - n)^{-2.2}$. Using this relation, an asteroid with 60% porosity survives 3.4× longer than an asteroid of the same size that has 30% porosity.

We note that any estimates of Q^* for porous asteroids are highly uncertain at present. It is not clear what strength measure should be used in relationships like equation (1). Equally uncertain is the range of event sizes over which target strength is important. In nonporous materials, a ratio of lithostatic pressure ρgR (ρ = target density, g = gravitational acceleration, R = asteroid radius) to the size-dependent tensile strength S is typically used to delineate the regimes where gravity or strength determine the outcome of a colli-

sion. Large or small values of ρgR/S indicate collisions in a gravity-dominated or strength-dominated regime respectively. Consider a similar approach for porous targets. There is reason to believe, based on as-yet-unpublished results by one of the authors (K.H.), that crushing strength provides a good correlation of cratering data for impacts into porous materials. In this case, a strength/gravity transition would be determined by the ratio $\rho gR/S_c$, where S_c is the crushing strength of the target material. Normally, a large value of this ratio would indicate a collision is gravity-dominated. However, by definition, a crushable material under the condition of $\rho gR/S_c \gg 1$ would self-compact until reaching a state near $\rho gR/S_c = 1$. On this basis, a gravity-dominated regime may never exist for collisions involving highly porous asteroids. Such bodies might always be restricted to a regime where strength is either dominant or, at best, comparable to lithostatic pressure. These questions must be studied further using both laboratory and numerical methods before reliable estimates of collisional lifetimes can be made.

5.4. Structure of Porous Asteroids

A large proportion of asteroids appear to have significant macroporosity, and in some cases the level of macroporosity suggests that the object has almost as much (or more) empty space within its volume as solid material. How can highly porous asteroids maintain so much empty macropore space? Spacecraft imaging of asteroid surfaces show that they are covered with a loose particulate regolith with particle sizes that are much smaller than the limit of resolution of the images (*Belton et al.,* 1995; *Veverka et al.,* 2000). In the case of the highest-resolution images of an asteroid surface, provided by the *NEAR Shoemaker* landing on 433 Eros, the finest surface material was again smaller than the limit of imaging resolution, suggesting dust-sized particles. But 433 Eros has an estimated macroporosity of 18%. Why doesn't this fine material filter into the interior cracks and voids and eliminate the object's macroporosity over time? As discussed in section 4, asteroid 253 Mathilde has an estimated macroporosity of 40%. Why doesn't the particulate material on the surface work its way into an object that is almost as much empty space as solid material? Can an asteroid maintain high internal porosity for what appears to be millions of years while meteoroid impacts on its surface grind down material to finer particle sizes, while shaking should cause that material to settle into pore spaces?

There are probably three major factors acting to create and preserve high levels of macroporosity in asteroids. First is the original structure of disrupted asteroids. When a previously coherent asteroid is catastrophically disrupted by a high-velocity impact, the physics of impacts favor a strong size sorting of the fragments that reaccrete. The largest disrupted pieces will have lowest relative velocities imparted by the collision and the largest relative gravitational attraction, so they will tend to be the ones to reaccrete first, forming an irregular core for the asteroid (*Melosh and Ryan,* 1997; *Wilson et al.,* 1999). Smaller size fractions would have progressively larger relative velocities, have smaller gravitational attractions, and take progressively longer to reaccrete. The tendency would be to size sort the rubble-pile asteroid with the largest (and most irregularly shaped) pieces in the center and progressively finer sizes building up in size-sorted layers. This size-sorted structure would create large void spaces in the interior of the asteroid while segregating the finer particle sizes on the outside layers of an asteroid.

The second factor is that in addition to the finest size fractions accreting last, the energy and processes that generate fine particles over time are impact-related regolith processes. These processes crush and pulverize asteroidal material, but necessarily operate only on the asteroid's surface. What is needed to fill the internal void space is a mechanism to move the fine material from the surface to the interior.

The third factor is the forces on those fine particles. Using a simple model of gravitational and frictional forces *Britt and Consolmagno* (2001) point out that while gravitational forces on particles increase linearly with the distance from the center of an object, the frictional forces preventing a piece of rubble from falling downward follow an inverse square law, increasing with the square of the depth into the body. While frictional force is weakest near the surface, it increases rapidly with depth. The small particles of the surface regolith tend to have the smallest gravitational force and a higher surface area to volume ratio than the larger particles; thus, they have proportionally the largest ratio of frictional to gravitational force. The smallest particles at any level are thus the ones most likely to be held up by friction. Calculations based on this model show that friction rapidly increases with depth and tends to quickly dominate gravitational force. For example, in a 40-km-diameter asteroid, frictional forces on a centimeter-sized particle would be 2 orders of magnitude larger than gravitational forces at only 10 m depth. By 500 m the difference is 4 orders of magnitude. The low gravitational acceleration on asteroids would also make it difficult for any particle to move a significant distance during the jolting and jostling that results from impact events. For example, for a 40-km-diameter asteroid, the gravitational acceleration at the surface is only 1.3 cm/s^2. For brief periods where interparticle contact is reduced or eliminated, this low acceleration would not allow much movement.

Another effect of friction may be to provide shattered bodies with what is in effect some level of coherent strength. Since friction will resist the displacement of the particles within a shattered object, pushing already-broken pieces apart would require larger forces than would be required by just gravitational scaling.

The implication is that for reaccreted rubble piles, the fine material generated and/or accreted at the surface tends to stay in the regolith zone. The major voids in the asteroid's deep interior that may date from the original reaccretion of the object remain unfilled. The major source of macroporosity reduction would probably come, as discussed earlier in this section, from the collapse of macroporosity due to major impacts. However, this is a very localized effect be-

cause of the rapid dissipation of the shock energy in the porous medium. Asteroid 253 Mathilde is an excellent example of an object with very high macroporosity that has survived repeated major impacts.

6. CONCLUSIONS AND FUTURE DIRECTIONS FOR ASTEROID POROSITY RESEARCH

6.1. Conclusions

Research into asteroid porosity and structure is still in its earliest stages. Shown in Fig. 1 are only 17 asteroids, some with substantial error bars. However, the rate of new asteroid bulk density measurements has increased remarkably over the last 10 years, and new measurements are being announced at every major planetary science meeting. This is an exciting time to see the density structure of the asteroid belt start to take shape. What we can interpret from these early and very limited data is extremely interesting:

1. Observations of asteroid mutual perturbation events, observations of asteroidal satellites (both optically and with radar), and spacecraft missions to asteroids have revolutionized our knowledge of asteroid bulk densities.

2. Meteorite studies have started to characterize the microporosity of meteorite groups. Using these data along with the grain density of meteorites, we can estimate bulk porosity and macroporosity of asteroids.

3. Most asteroids tend to have significant bulk porosity and significant macroporosity.

4. The three asteroids with diameters >500 km are coherent objects without macroporosity. Other than these three, low-macroporosity asteroids are rare.

5. A group of asteroids, including 433 Eros, have macroporosities of ~20%. These moderate-macroporosity asteroids have probably been significantly fractured, but not collisionally disrupted. Alternately, if they were disrupted and reassembled, they must have experienced significant compression by subsequent impacts.

6. A group of asteroids, including 253 Mathilde, have macroporosities >30% and in some cases >50%. These objects are probably loosely consolidated piles of collisional rubble whose internal structure is highly porous.

7. C-type asteroids tend to have greater macroporosities than S-type asteroids, suggesting that S-type asteroids are somewhat more resistant to catastrophic disruption, but both types are represented in the different groups.

8. Asteroids can have substantial interior macroporosity while retaining a fine loose surface regolith. Fine particle size fractions tend to be accreted and/or generated at the surface of an asteroid, but frictional and not gravitational forces dominate the movement of small particles, preventing infilling fractures and voids within the object.

9. High macroporosity creates a different and unusual impact regime in asteroids. Effects include rapid attenuation of shock, low-ejecta velocities, crater formation by compaction rather than ejection of material, and significantly enhanced survival against impacts that would otherwise disrupt a coherent object of the same size.

6.2. Future Directions

The little that is known about asteroid porosity whets the appetite for more knowledge and hints at exciting areas of research. First and foremost is the need for continuing observations of asteroids, both for mutual perturbation events and discovering satellites. Most of the mutual event and satellite data come from relatively large asteroids (i.e., masses $>10^{18}$ kg) and the figures of this paper are sparsely populated with asteroids less than that mass. Observations of asteroids a few hundred meters in diameter are only now becoming available, albeit with large error bars. Also needed are more porosity measurements of meteorites. Ordinary chondrites have been well characterized, but the surface has only been scratched on the other meteorite groups and a number of major questions remain to be answered.

The impact physics of porous asteroids is perhaps the most significant frontier. Porous targets appear to dominate the asteroid belt, but very little is known about how the nature of those targets affects the processes and outcomes of impacts. What we do know is that porosity does have a major effect on these processes and outcomes as illustrated by the images of 253 Mathilde that show at least five impact craters that should be large enough to disrupt a coherent object. With more measurements of asteroids and meteorites, and a greater understanding of the physics of impacts into porous targets, our understanding of the internal structure of asteroids will greatly expand. Already with our limited data we can see: an asteroid belt that contains large, coherent asteroids coexisting with somewhat smaller, shattered rubble piles; asteroids of the same spectral type and therefore similar mineralogy with factors of 3 differences in their bulk densities; and asteroids with more empty space than solid material. It is clear that the asteroid belt is a very interesting place, full of surprises and intellectual adventures.

REFERENCES

Asphaug E., Ostro S. J., Hudson R. S., Scheeres D. J., and Benz W. (1998) Disruption of kilometre-sized asteroids by energetic collisions. *Nature, 393,* 437–440.

Asphaug E., Ryan E. V., and Zuber M. T. (2002) Asteroid interiors. In *Asteroids III* (W. F. Bottke Jr. et al., eds.), this volume. Univ. of Arizona, Tucson.

Bange J. (1998) An estimation of the mass of asteroid 20-Massalia derived from the Hipparcos minor planets data. *Astron. Astrophys., 340,* L1–L4.

Belton M. J. S., Chapman C. R., Thomas P. C., Davies M. E., Greenberg R., Klassen K., Byrnes D., D'Amario L., Synnott S., Johnson T. V., McEwen A., Merline M. J., Davis D. R., Petit J.-M., Storrs A., Veverka J., and Zellner B. (1995) Bulk density of asteroid 243 Ida from the orbit of its satellite Dactyl. *Nature, 374,* 785–788.

Benner L. A. M., Ostro S. J., Giorgini J. D., Jurgens R. F., Margot J. L., and Nolan M. C. (2001) *1999 KW4; N Aql 2001.* IAU Circular 7632.

Bland P. A., Sexton A. S., Jull A. J. T., Bevan A. W. R., Berry F. J., Thornley D. M., Astin T. R., Britt D. T., and Pillinger C. T. (1998) Climate and rock weathering: A study of terrestrial age dated ordinary chondritic meteorites from hot desert

regions. *Geochim. Cosmochim. Acta, 62,* 3169–3184.
Bottke W. F., Nolan M. C., Kolvoor R. A., and Greenberg R. (1994) Velocity distribution among colliding asteroids. *Icarus, 107,* 255–268.
Britt D. T. and Consolmagno G. J. (2000) The porosity of dark meteorites and the structure of low-albedo asteroids. *Icarus, 146,* 213–219.
Britt D. T. and Consolmagno G. J. (2001) Modeling the structure of high-porosity asteroids. *Icarus, 152,* 134–139.
Chapman C. R., Merline W. J., and Thomas P. (1999) Cratering on Mathilde. *Icarus, 140,* 28–33.
Consolmagno G. J. and Britt D. T. (1998) The density and porosity of meteorites from the Vatican collection. *Meteoritics & Planet. Sci., 33,* 1231–1242.
Consolmagno G. J., Britt D. T., and Stoll C. P. (1998) The porosities of ordinary chondrites: Models and interpretation. *Meteoritics & Planet. Sci., 33,* 1221–1230.
Consolmagno G. J., Bland P. A., and Strait M. M. (1999) Weathering and porosity: A preliminary SEM study of weathered meteorites (abstract). In *Lunar and Planetary Science XXX,* Abstract #1158. Lunar and Planetary Institute, Houston (CD-ROM).
Drummond J. D. and Cocke W. J. (1989) Triaxial ellipsoid dimensions and rotational pole of 2 Pallas from two stellar occultations. *Icarus, 78,* 323–329.
Drummond J. D., Fugate R. Q., Christou J. C., and Hege E. K. (1998) Full adaptive optics images of asteroids Ceres and Vesta; rotational poles and triaxial ellipsoid dimensions. *Icarus, 132,* 80–99.
Dunham D. W. and 45 colleagues (1990) The size and shape of (2) Pallas from the 1983 occultation of 1 Vulpeculae. *Astron. J., 99,* 1636–1662.
Farinella P. and Davis D. R. (1994) Will the real size distribution please step forward? (abstract). In *Lunar and Planetary Science XXV,* pp. 365–366. Lunar and Planetary Institute, Houston.
Flynn G. J., Moore L. B., and Klock W. (1999) Density and porosity of stone meteorites: Implications for the density, porosity, cratering, and collisional disruption of asteroids. *Icarus, 142,* 97–105.
Gaffey M. J., Bell J. F., Brown R. H., Burbine T. H., Piatek J. L., Reed K., and Chaky D. A. (1993) Mineralogical variations within the S-type asteroid class. *Icarus, 106,* 573–602.
Grady M. M. (2000) *Catalogue of Meteorites,* 5th edition. Cambridge Univ., Cambridge. 696 pp.
Goffin E. (1991) The orbit of 203 Pompeja and the mass of Ceres. *Astron. Astrophys., 249,* 563–568.
Goffin E. (2001) New determination of the mass of Pallas. *Astron. Astrophys., 365,* 627–630.
Hagerty M. M., Hite D. R., Ulrich C. R., and Hagerty D. J. (1993) One-dimensional high pressure compression of granular media. *J. Geotech. Eng., 119,* 1–18.
Hertz H. (1966) *T Pyx; 1966e; The Mass of Vesta; Notice Re. Precise Positions of Comets.* IAU Circular 1983 (see also *Science, 160,* 299–300).
Hilton J. L. (1997) The mass of the asteroid 15 Eunomia from observations of 1313 Berna and 1284 Latvia. *Astron. J., 114,* 402–408.
Hilton J. L. (1999) US Naval Observatory ephemerides of the largest asteroids. *Astron. J., 117,* 1077–1086.
Hilton J. L. (2002) Asteroid masses and densities. In *Asteroids III* (W. F. Bottke Jr. et al., eds.), this volume. Univ. of Arizona, Tucson.
Hilton J. L., Seidelmann P. K., and Middour J. (1996) Prospects for determining asteroid masses. *Astron. J., 112,* 2319–2329.
Holsapple K. A. (1993) The scaling of impact processes in planetary sciences. *Annu. Rev. Earth Planet. Sci., 21,* 333–373.
Holsapple K., Giblin I., Housen K., Nakamura A., and Ryan E. (2002) Asteroid impacts: Laboratory experiments and scaling laws. In *Asteroids III* (W. F. Bottke Jr. et al., eds.), this volume. Univ. of Arizona, Tucson.
Housen K. R. and Holsapple K. A. (1999) Scale effects in strength-dominated collisions of rocky asteroids. *Icarus*, *142,* 21–33.
Housen K. R. and Voss M. E. (2001) Ejecta from impact craters in porous materials (abstract). In *Lunar and Planetary Science XXXII,* Abstract #1617. Lunar and Planetary Institute, Houston (CD-ROM).
Housen K. R., Holsapple K. A., and Voss M. E. (1999) Compaction as the origin of the unusual craters on asteroid Mathilde. *Nature, 402,* 155–157.
Lambe T. W. and Whitman R. V. (1969) *Soil Mechanics.* Wiley and Sons, New York. 553 pp.
Landgraf W. (1988) The mass of Ceres. *Astron. Astrophys., 191,* 161–166.
Landgraf W. (1992) A determination of the mass of (704) Interamnia from observations of (993) Moultona. In *Chaos, Resonance, and Collective Dynamical Phenomena in the Solar System* (S. Ferraz-Mello, ed.), pp. 179–182. Kluwer, Dordrecht.
Lopez Garcia A., Medvedev Yu. D., and Morano Fernandez J. A. (1997) Using close encounters of minor planets for the improvement of their masses. In *Dynamics and Astrometry of Natural and Artificial Celestial Bodies* (I. M. Wytrzyszczak et al., eds.), pp. 199–204. Kluwer, Dordrecht.
Love S. J., Hörz F., and Brownlee D. E. (1993) Target porosity effects in impact cratering and collisional disruption. *Icarus, 105,* 216–224.
Lundborg N. (1967) The strength-size relation of granite. *Intl. J. Rock Mech. Min. Sci., 4,* 269–272.
Margot J. L. and Brown M. E. (2001) Discovery and characterization of binary asteroids 22 Kalliope and 87 Sylvia. *Bull. Am. Astron. Soc., 33,* 1133.
Margot J. L., Nolan M. C., Benner L. A., Ostro S. J., Jurgens R. F., Giorgini J. D., Slade M. A., and Campbell D. B. (2001) Radar observations of binary asteroid 2000 DP107 (abstract). In *Lunar and Planetary Science XXXII,* Abstract #1754. Lunar and Planetary Institute, Houston (CD-ROM).
McSween H. Y. (1999) *Meteorites and Their Parent Planets.* Cambridge Univ., New York. 310 pp.
Meibom A. and Clark B. E. (1999) Evidence for the insignificance of ordinary chondritic material in the asteroid belt. *Meteoritics & Planet. Sci., 34,* 7–24.
Melosh H. J. and Ryan E. V. (1997) Asteroids: Shattered but not dispersed. *Icarus, 129,* 562–564.
Menikoff R. (2001) Meso-scale simulations of compaction waves in granular beds. *23rd Intl. Symp. Shock Waves,* Paper #5016. Fort Worth, Texas.
Merline W. J., Close L. M., Dumas C., Chapman C. R., Roddler F., Menard F., Slater D. C., Duvert G., Shelton C., and Morgan T. (1999) Discovery of a moon orbiting the asteroid 45 Eugenia. *Nature, 401,* 565–568.
Merline W. J., Close L. M., Dumas C., Shelton J. C., Menard F., Chapman C. R., and Slater D. C. (2000) Discovery of companions to asteroids 762 Pulcova and 90 Antiope by direct imaging. *Bull. Am. Astron. Soc., 32,* 1017.
Michalak G. (2000) Determination of asteroid masses I. (1) Ceres, (2) Pallas and (4) Vesta. *Astron. Astrophys., 360,* 363–374.
Millis R. L. and 41 colleagues (1987) The size, shape, density, and albedo of Ceres from its occultation of BD+8o471. *Icarus,*

72, 507–518.

Nakamura A., Suguiyama K., and Fujiwara A. (1992) Velocity and spin of fragments from impact disruptions. I. An experimental approach to a general law between mass and velocity. *Icarus, 100,* 127–135.

Nolan M. C., Margot J.-L., Howell E. S., Benner L. A. M., Ostro S. J., Jurgens R. F., Giorgini J. D., and Campbell D. B. (2001) Radar observations of near-Earth asteroids 2000 UG11 and 2000 UK11 (abstract). In *Lunar and Planetary Science XXXII,* Abstract #2055. Lunar and Planetary Institute, Houston (CD-ROM).

Richardson D. C., Leinhardt Z. M., Melosh H. J., Bottke W. F. Jr., and Asphaug E. (2002) Gravitational aggregates: Evidence and evolution. In *Asteroids III* (W. F. Bottke Jr. et al., eds.), this volume. Univ. of Arizona, Tucson.

Ryan E. V., Davis D. R., and Giblin I. (1999) A laboratory impact study of simulated Edgeworth-Kuiper belt objects. *Icarus, 142,* 56–62.

Sears D. W. G. (1998) The case for rarity of chondrules and calcium-aluminum-rich inclusions in the early solar system and some implications for astrophysical models. *Astrophys. J., 498,* 773–778.

Scholl H., Schmadel L.D., and Roeser S. (1987) The mass of the asteroid (10) Hygiea derived from observations of (829) Academia. *Astron. Astrophys., 179,* 311–316.

Schubart J. and Matson D. L. (1979) Masses and densities of asteroids. In *Asteroids* (T. Gehrels, ed.), pp. 84–97. Univ. of Arizona, Tucson.

Standish E. M. (1998) JPL Planetary and Lunar Ephemerides, DE405/LE405. *JPL Interoffice Memorandum 312.F-98-048,* August 26, 1998.

Standish E. M. (2001) *JPL Interoffice Memorandum 312.F-01-006,* April 11, 2001.

Standish E. M. and Hellings R.W. (1989) A determination of the masses of Ceres, Pallas, and Vesta from their perturbations on the orbit of Mars. *Icarus, 80,* 326–333.

Stewart S. and Ahrens T. J. (1999) Porosity effects on impact processes in solar system materials (abstract). In *Lunar and Planetary Science XXXI,* Abstract #2020. Lunar and Planetary Institute, Houston (CD-ROM).

Tedesco E. F. (1989) Asteroid magnitudes, UBV colors, and IRAS albedos and diameters. In *Asteroids II* (R. P. Binzel et al., eds.), pp. 1090–1150. Univ. of Arizona, Tucson.

Tedesco E. F., Veeder G. J., Fowler J. W., and Chillemi J. R. (1992) *The IRAS Minor Planet Survey.* Phillips Laboratory Report PL-TR-92-2049.

Terho M., Pesonen L. J., Kukkonen I. T., and Bukovansk M. (1993) The petrophysical classification of meteorites. *Studia Geoph. Geod., 37,* 65–82.

Thomas P. C., Binzel R. P., Gaffey M. J., Storrs A. D., Wells E. N., and Zellner B. H. (1997) Impact excavation on asteroid 4 Vesta: Hubble Space Telescope results. *Science, 277,* 1492–1495.

Veillet C., Doressoundiram A., and Shapiro J. (2001) *S/2000 (1998 WW31) 1.* IAU Circular 7610.

Veverka J., Thomas P., Harch A., Clark B., Bell J. F. III, Carcich B., Joseph J., Chapman C., Merline W., Robinson M., Malin M., McFadden L. A., Murchie S., Hawkins S. E. III, Farquhar R., Izenberg N., and Cheng A. (1997) NEAR's flyby of 253 Mathilde: Images of a C asteroid. *Science, 278,* 2109–2114.

Veverka J., Robinson M., Thomas P., Murchie S., Bell J. F. III, Izenberg N., Chapman C., Harch A., Bell M., Carcich B., Cheng A., Clark B., Domingue D., Dunham D., Farquhar R., Gaffey M. J., Hawkins E., Joseph J., Kirk R., Li H., Lucey P., Malin M., Martin P., McFadden L., Merline W. J., Miller J. K., Owen W. M. Jr., Peterson C., Prockter L., Warren J., Wellnitz D., Williams B. G., and Yeomans D. K. (2000) NEAR at Eros: Imaging and spectral results. *Science, 289,* 2088–2097.

Viateau B. (2000) Mass and density of asteroids (16) Psyche and (121) Hermione. *Astron. Astrophys., 354,* 725–731.

Viateau B. and Rapaport M. (1995) The orbit of (2) Pallas. *Astron. Astrophys. Suppl. Ser., 111,* 305–310.

Viateau B. and Rapaport M. (1997) The Bordeaux meridian observations of asteroids. First determination of the mass of (11) Parthenope. *Astron. Astrophys., 320,* 652–658.

Viateau B. and Rapaport M. (1998) The mass of (1) Ceres from its gravitational perturbations on the orbits of 9 asteroids. *Astron. Astrophys., 334,* 729–735.

Wasserman L. H., Millis R. L., Franz O. G., Bowell E., White N. M., Giclas H. L., Martin L. J., Elliot J. L., Dunham E., Mink D., Baron R., Honeycutt R. K., Henden A. A., Kephart J. E., A'Hearn M. F., Reitsema H. J., Radick R., and Taylor G. E. (1979) The diameter of Pallas from its occultation of SAO 85009. *Astron. J., 84,* 259–268.

Weidenshilling S. J., Marzari F., Davis D. R., and Neese C. (2001) Origin of the double asteroid 90 Antiope: A continuing puzzle (abstract). In *Lunar and Planetary Science XXXII,* Abstract #1890. Lunar and Planetary Institute, Houston (CD-ROM).

Wilkison S. L. and Robinson M. S. (2000) Bulk density of ordinary chondrite meteorites and implications for asteroidal internal structure. *Meteoritics & Planet. Sci., 35,* 1203–1213.

Wilson L., Keil K., and Love S. J. (1999) The internal structures and densities of asteroids. *Meteoritics & Planet. Sci., 34,* 479–483.

Yamamuro J. A., Bopp P. A., and Lade P. V. (1996) One-dimensional compression of sands at high pressures. *J. Geotech. Eng., 121,* 147–155.

Yeomans D. K., Barriot J.-P., Dunham D. W., Farquhar R. W., Giorgini J. D., Helfrich C. E., Konopliv A. S., McAdams J. V., Miller J. K., Owen W. M. Jr., Scheeres D. J., Synnott S. P., and Williams B. G. (1997) Estimating the mass of asteroid 253 Mathilde from tracking data during the NEAR flyby. *Science, 278,* 2106–2109.

Yeomans D. K., Antreasian P. G., Cheng A., Dunham D. W., Farquhar R. W., Gaskell R. W., Giorgini J. D., Helfrich C. E., Konopliv A. S., McAdams J. V., Miller J. K., Owen W. M. Jr., Thomas P. C., Veverka J., and Williams B. G. (1999) Estimating the mass of asteroid Eros during the NEAR spacecraft flyby. *Science, 285,* 560–561.

Yeomans D. K., Antreasian P. G., Barriot J.-P., Chesley S. R., Dunham D. W., Farquhar R. W., Giorgini J. D., Helfrich C. E., Konopliv A. S., McAdams J. V., Miller J. K., Owen W. M. Jr., Scheeres D. J., Thomas P. C., Veverka J., and Williams B. G. (2000) Radio science results during the NEAR Shoemaker spacecraft rendezvous with Eros. *Science, 289,* 2085–2088.

Zuber M. T., Smith D. E., Cheng A. F., Garvin J. B., Aharonson O., Cole T. D., Dunn P. J., Guo Y., Lemoine F. G., Neumann G. A., Rowlands D. D., and Torrence M. H. (2000). The shape of 433 Eros for the NEAR Shoemaker laser rangefinder. *Science, 289,* 2097–2101.